The Effects of North Atlantic SST and Sea Ice Anomalies on the Winter Circulation in CCM3. Part II: Direct and Indirect Components of the Response

CLARA DESER

National Center for Atmospheric Research, Boulder, Colorado*

GUDRUN MAGNUSDOTTIR

Department of Earth System Science, University of California, Irvine, Irvine, California

R. SARAVANAN AND ADAM PHILLIPS

National Center for Atmospheric Research, Boulder, Colorado*

(Manuscript received 16 January 2003, in final form 6 October 2003)

ABSTRACT

The wintertime atmospheric circulation responses to observed patterns of North Atlantic sea surface temperature and sea ice cover trends in recent decades are studied by means of experiments with an atmospheric general circulation model. Here the relationship between the forced responses and the dominant pattern of internally generated atmospheric variability is focused on. The total response is partioned into a portion that projects onto the leading mode of internal variability (the indirect response) and a portion that is the residual from that projection (the direct response). This empirical decomposition yields physically meaningful patterns whose distinctive horizontal and vertical structures imply different governing mechanisms. The indirect response, which dominates the total geopotential height response, is hemispheric in scale with resemblance to the North Atlantic Oscillation or Northern Hemisphere annular mode, and equivalent barotropic in the vertical from the surface to the tropopause. In contrast, the direct response is localized to the vicinity of the surface thermal anomaly (SST or sea ice) and exhibits a baroclinic structure in the vertical, with a surface trough and upper-level ridge in the case of a positive heating anomaly, consistent with theoretical models of the linear baroclinic response to extratropical thermal forcing. Both components of the response scale linearly with respect to the amplitude of the forcing but nonlinearly with respect to the polarity of the forcing. The deeper vertical penetration of anomalous heating compared to cooling is suggested to play a role in the nonlinearity of the response to SST forcing.

1. Introduction

Sea surface temperature (SST) and sea ice cover in the North Atlantic have undergone pronounced trends in recent decades. Although driven in large part by changes in atmospheric flow (cf. Deser et al. 2000; Seager et al. 2000), the trends in SST and sea ice may exert a significant feedback upon the atmospheric circulation. The nature of this feedback is the subject of the present study and a companion study (Magnusdottir et al. 2004, hereafter referred to as Part I). In this work, we examine the wintertime atmospheric circulation responses to observed patterns of North Atlantic SST and sea ice cover trends by means of experiments with an atmospheric general circulation model, version 3 of the Community Climate Model (CCM3). As shown in Part I, a notable result of these experiments is the similarity of the response to trends in ice cover and to trends (with reversed sign) in SST, despite large differences in the spatial pattern and amplitude of the two forcing parameters. In addition, these responses resemble the model's leading mode of internal variability, the simulated equivalent of the observed North Atlantic Oscillation or Northern Hemisphere annular mode patterns (e.g., Wallace 2000). Previous modeling studies have also found a correspondence between the patterns of internal variability and the response to an imposed midlatitude heating perturbation (Peng and Robinson 2001; Hall et al. 2001) or to increasing greenhouse gas concentrations (Kushner et al. 2001).

The purpose of Part II of this study is to further examine the relationship between the forced response to trends in SST and sea ice cover, and the dominant pat-

*The National Center for Atmospheric Research is sponsored by the National Science Foundation.

Corresponding author address: Dr. Clara Deser, Climate and Global Dynamics Division, NCAR, P.O. Box 3000, Boulder, CO 80307-3000.
E-mail: cdeser@ucar.edu

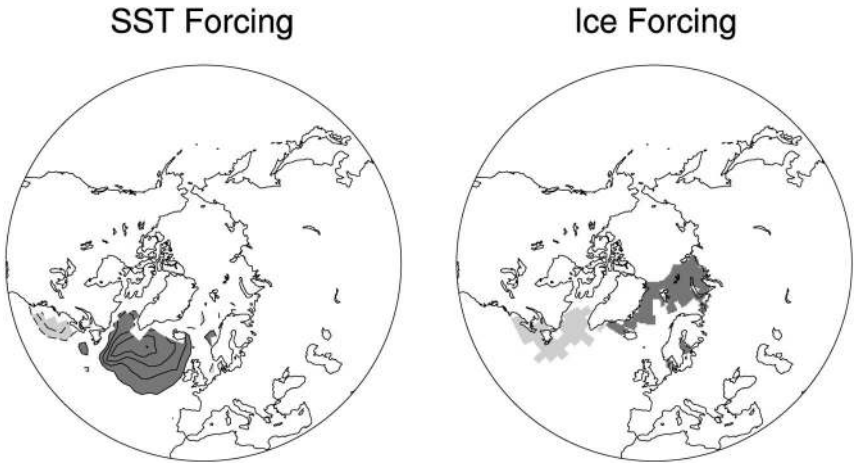

FIG. 1. Jan (left) SST and (right) sea ice forcing used in the SST−5 and ICE2 perturbation experiments, respectively. In the SST panel, dark (light) shading denotes positive (negative) anomalies relative to the control run; the contour interval is 1.5 K and the zero contour has been omitted. In the sea ice panel, dark (light) shading denotes grid boxes where sea ice has been removed (added) relative to the control run.

tern of internally generated atmospheric variability. Specifically, we partition the total geopotential height response into a portion that projects onto the leading mode of internal variability (the indirect response) and the residual from that projection (the direct response). This empirical decomposition is shown to yield physically meaningful patterns whose distinctive horizontal and vertical structures imply different governing mechanisms. Kushner et al. (2001) also found such an approach insightful for understanding the zonally averaged atmospheric circulation response in the Southern Hemisphere to increasing greenhouse gas concentrations in a coupled climate model.

It was noted in Part I that the total geopotential height response to trends in SST and sea ice is nonlinear with respect to the polarity of the forcing. Here we expand upon this issue by examining the sensitivity of both the direct and indirect components of the response to the sign of the imposed SST and sea ice anomaly trends. We also investigate the vertical distribution of anomalous heating compared to cooling in these experiments, a factor which may play a role in the nonlinearity of the response.

The outline of the paper is as follows. Section 2 provides a brief overview of the experiments analyzed. Section 3 presents the decomposition of the total geopotential height response into direct and indirect components, and documents the vertical distribution of anomalous heating associated with the imposed SST and sea ice anomaly trends. Section 4 discusses and summarizes the results.

2. Experimental design

A complete description of the atmospheric general circulation model (CCM3) and experimental design is given in Part I. The two primary experiments analyzed here are termed SST−5 and ICE2. In SST−5, the forcing is defined as the observed monthly SST anomaly trend during 1954–94 over the North Atlantic, multiplied by a factor of −5 (i.e., the polarity of the observed trend is reversed and its amplitude is magnified fivefold). In ICE2, the forcing is the observed monthly trend in sea ice extent over the North Atlantic during 1958–97, magnified by approximately a factor of 2. In each case, the forcing is applied as an anomaly upon the mean seasonal cycle. Each experiment, as well as a control simulation forced with the climatological seasonal cycle of SST and sea ice cover, is integrated for a minimum of 61 yr; we analyze years 2–61 from each run.

Figure 1 shows the January SST and sea ice anomalies in SST−5 and ICE2, respectively; anomalies in the other winter months are similar (not shown). In SST−5, the primary forcing is a positive SST anomaly center located in the subpolar gyre (maximum amplitude ~7 K), with a weaker negative anomaly off the east coast of North America (maximum amplitude ~3 K). In ICE2, the forcing consists of a reduction in sea ice cover in the Greenland Sea and an extension of the ice edge in the Labrador Sea. Note that a grid cell is either ice free or 100% ice covered; there is no fractional ice concentration.

We shall also make use of additional experiments that have been conducted to test the sensitivity of the response to the magnitude and polarity of the imposed thermal forcing. For SST forcing, these are termed SST+5, SST+2.5, and SST−2.5; for sea ice forcing these are ICE1, ICELAB, and ICEGRN. SST+5 is identical to SST−5 except for a sign reversal (e.g., the observed SST trend magnified by a factor of 5); SST+2.5 (SST−2.5) is identical to SST+5 (SST−5) except that the observed trend is multiplied by a factor of 2.5

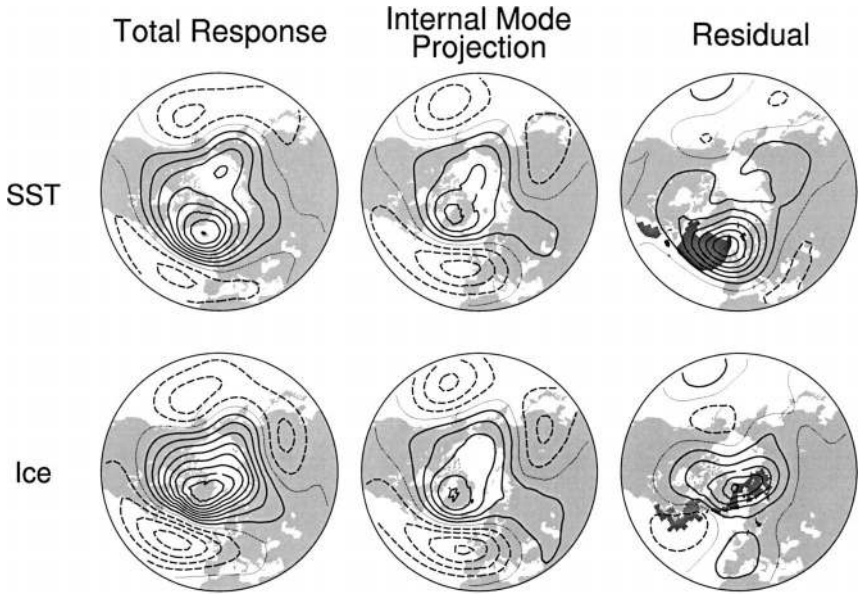

FIG. 2. Decomposition of the (left) total Dec–Apr Z_{500} responses in (top) SST−5 and (bottom) ICE2 into a component that projects onto the leading EOF of (middle) the control run and (right) the residual from that projection. The contour interval is 10 m in all panels; positive (negative) contours are solid (dashed) and the zero contour is the thin solid line. The locations of the SST and sea ice anomalies are indicated by shading in the residual panels.

(−2.5); ICE1 is identical to ICE2 except that the areal extent of the observed sea ice trend has not been magnified; ICELAB (ICEGRN) is identical to ICE2 except that only the Labrador (Greenland) Sea portion of the sea ice cover is altered.

3. Results

a. Geopotential height response

The left-hand panels of Fig. 2 show the total geopotential height response at 500 hPa (Z_{500}) for the winter season December–April for SST−5 and ICE2, obtained by subtracting the 60-yr mean of the control simulation from the 60-yr mean of each perturbation experiment (April is included in the definition of winter due to the strong similarity between the March and April responses in both experiments; not shown). Values exceeding approximately 10 m in absolute value are significant at the 95% confidence level according to a local *t* test (not shown). Although the SST and sea ice forcings differ in location and magnitude, the responses are remarkably similar in both amplitude and spatial pattern. Both response patterns are hemispheric in nature (although the forcing is confined to the Atlantic sector), with positive height anomalies at high latitudes and negative height anomalies at midlatitudes of the Atlantic and Pacific. Maximum height anomalies are ~80 m in the polar region and ~−(20–40 m) in midlatitudes.

As noted in the introduction, there is an emerging consensus that the internal variability in an atmospheric general circulation model may play a strong role in shaping the pattern of the forced response. The middle panels of Fig. 2 show the leading EOF of winter Z_{500} from the control run, which accounts for 33% of the variance (and is well separated from the second EOF) over the Northern Hemisphere north of 30°N. Cosine weighting has been used in the covariance matrix to compute the EOF. (The scaling of the EOF patterns, which differs slightly in the two middle panels, is described shortly.) The similarity between the leading EOF of the control run and the response patterns in both experiments is evident: the pattern correlation is 0.70 for SST−5 and 0.84 for ICE2. The principal component time series for the control run EOF is approximately normally distributed about a mean of zero (not shown but see Part I).

Although there is a high degree of similarity between the leading Z_{500} EOF in the control run and the Z_{500} responses in the two experiments, there are some subtle distinctions in the relative amplitude and location of the centers of action. To examine these differences, we projected the response onto the EOF using linear least squares spatial regression, and then subtracted the projection (the EOF scaled by the regression coefficient: middle panels of Fig. 2) from the response to obtain the residual. We excluded the forcing region (90°W–45°E) from the calculation of the spatial regression coefficient so as to optimally compare the features of the far-field response that are common to the internal variability; however, similar results are obtained when the full hemispheric domain is used (not shown). In both experiments, the total response is dominated by its projection onto the internal variability; however, a well-defined

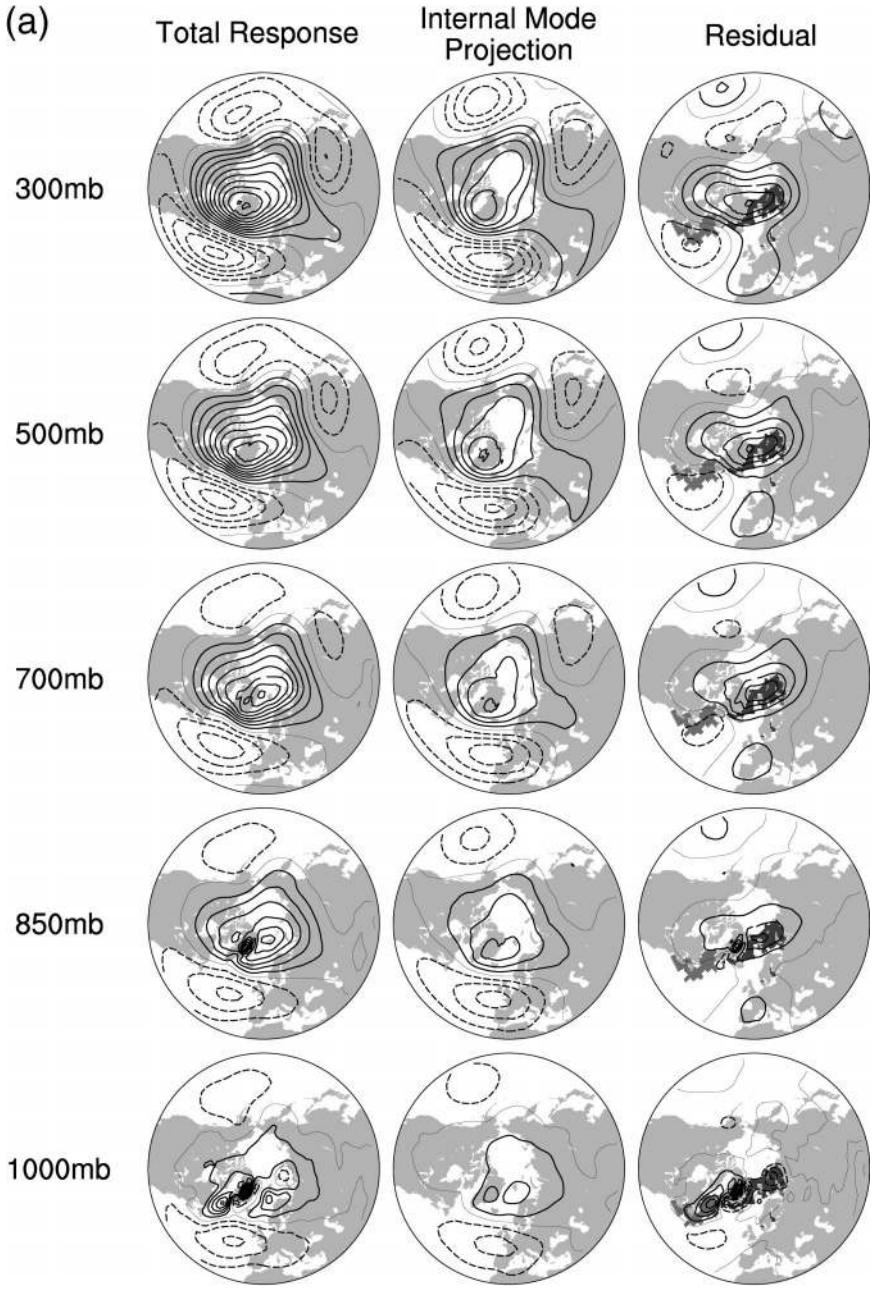

FIG. 3. As in Fig. 2 but for different levels in the troposphere: (a) ICE2, (b) SST−5, and (c) SST+5.

residual pattern that is closely tied to the location of the forcing is also apparent (right-hand panels of Fig. 2). In SST−5, the residual response consists of an anomalous ridge over and slightly downstream of the warm SST anomaly, with maximum amplitude ~60 m (10 m K^{-1}). In ICE2, the main feature of the residual response is an anomalous ridge centered over the Greenland Sea in the region of sea ice removal and extending over the polar cap, with maximum amplitude ~50 m. The anomalous ridge response in the residual fields in both experiments is consistent with simple physical reasoning (e.g., a raising of geopotential height surfaces within and above an anomalously warm column of air), lending credence to our diagnostic technique and the notion that the total response may be partitioned into direct (e.g., residual) and indirect (e.g., projection onto the leading mode of internal variability) components. We note that neither residual pattern resembles any of the higher-order EOFs in the control run, suggesting that the residual is indeed a direct, forced response.

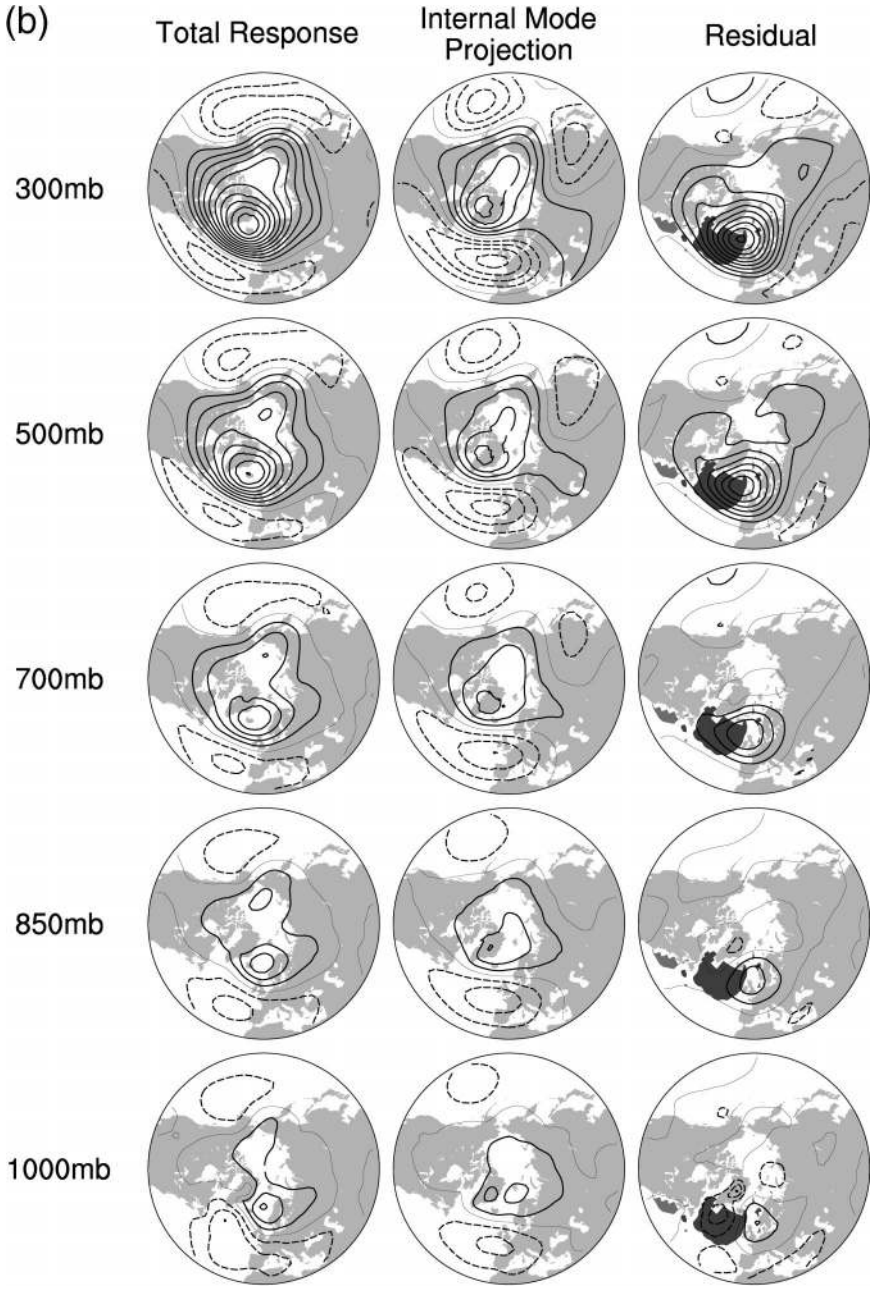

FIG. 3. (*Continued*)

The vertical structures of the total, indirect, and direct responses are shown in Fig. 3. The indirect responses were computed by regressing the geopotential height anomalies (relative to the 60-yr mean) in the control run at each level upon the leading 500-hPa principal component time series in the control run, and then scaling those regression patterns (denoted Z_{reg}) by the spatial regression coefficient between the total height response (experiment-minus-control) and Z_{reg} at each level separately. In this way, we ensure that the indirect responses shown in Fig. 3 represent the projections upon a single mode of internal variability as represented by the leading PC time series at 500 hPa. However, using the leading EOF computed separately for each level in the control run in place of Z_{reg} yields nearly identical results due to the high temporal correlation (>0.96) between the leading PC time series at each level with that at 500 hPa (not shown).

For ICE2 (Fig. 3a), the vertical structure of the total response pattern is approximately equivalent barotropic,

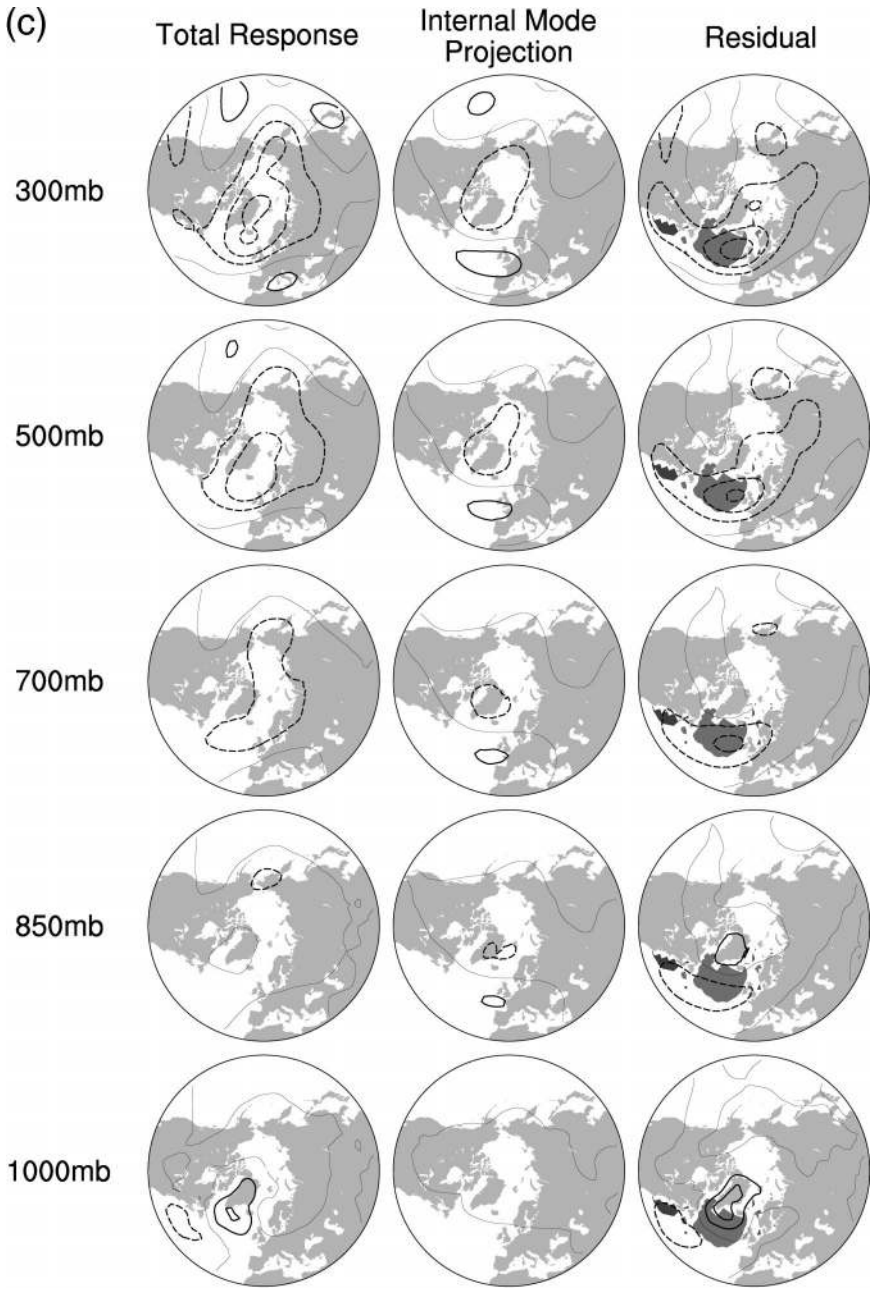

FIG. 3. (*Continued*)

with embedded small-scale structures evident at 1000 hPa coincident with the location of the sea ice anomalies. The indirect response is also equivalent barotropic, as expected and consistent with previous studies (e.g., Ting and Lau 1993). Note the absence of localized ice-related structures in the indirect response at 1000 hPa. The direct response is baroclinic between 1000 and 850 hPa over the regions of anomalous sea ice cover; for example, where sea ice has been removed in the Greenland Sea, the height anomalies are negative at 1000 hPa and positive at 850 hPa, indicative of a local warming of the boundary layer. Above the boundary layer, the direct response consists of a primary center of above normal heights over the Greenland Sea and spreading to much of the Arctic. This anomalous ridge grows with height from 850 to 500 hPa, with no further amplification between 500 and 300 hPa. A weaker anomalous trough is also present over and downstream of the enhanced ice cover in the Labrador Sea.

For SST−5 (Fig. 3b), the vertical structures of the

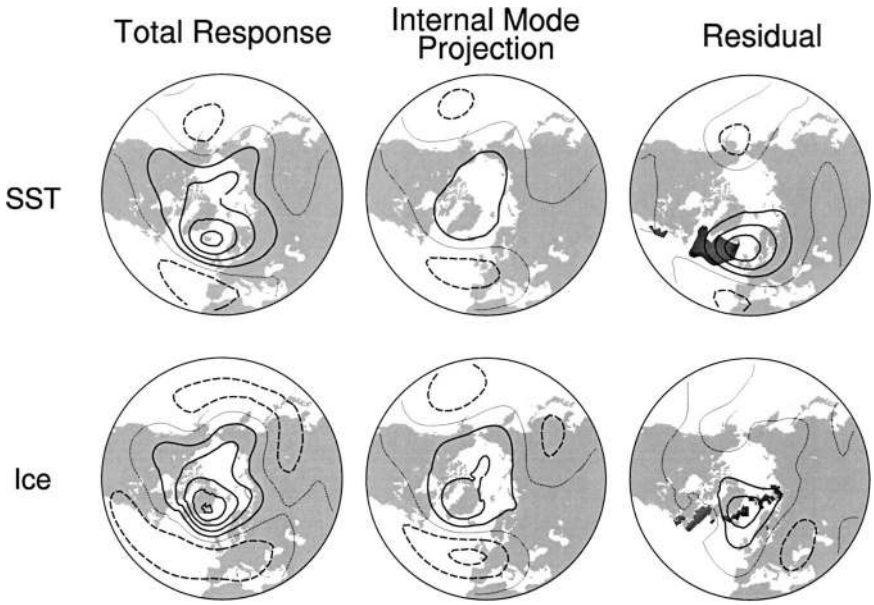

FIG. 4. As in Fig. 2 but for (top) SST−2.5 and (bottom) ICE1.

total and indirect responses are approximately equivalent barotropic, similar to those for ICE2. The residual response is baroclinic within the boundary layer directly over the positive SST anomaly (i.e., an anomalous trough at 1000 hPa and near-zero height anomalies at 850 hPa), also similar to the results for ICE2. The residual response in the free atmosphere consists of an equivalent barotropic anomalous ridge over and downstream of the warm SST anomaly. Note that this anomalous ridge amplifies considerably between 500 and 300 hPa, unlike the corresponding feature in ICE2, which attains its maximum amplitude at 500 hPa.

We have also carried out the decomposition for ICEGRN, ICELAB, and SST+5. The total, indirect, and direct responses for ICEGRN (not shown) are very similar to those for ICE2 (except for the lack of a local boundary layer response over the Labrador Sea due to the absence of sea ice forcing there), while the ICELAB responses (not shown) are weak and not statistically significant (except for the boundary layer response over the Labrador Sea). These results indicate that it is the removal of sea ice in the Greenland Sea rather than the addition of sea ice in the Labrador Sea that is primarily responsible for the circulation response in ICE2 (see also Part I).

The total, indirect, and direct responses for SST+5 are shown in Fig. 3c. While similar in spatial and vertical structure (albeit with opposite sign) to their SST−5 counterparts, their magnitudes are considerably weaker. For example, the amplitudes of the total and indirect responses throughout the troposphere are approximately a factor of 3 smaller for SST+5 than SST−5. In addition, the anomalous trough in the direct free-atmosphere response to SST+5 exhibits less amplification with height than the analogous ridge in SST−5: the magnitude of the maximum height anomaly at 300 hPa is ~30 m in SST+5 compared to ~90 m in SST−5. The fact that our empirical technique for decomposing the total response yields meaningful patterns even for the small amplitude response in SST+5 lends further support to its credibility.

In summary, the total response to positive surface temperature anomalies, either in the form of SST changes or reductions in sea ice cover, is dominated by the spatial (hemispheric) and vertical (approximately equivalent barotropic) structure of the leading mode of internal variability of the model's wintertime atmospheric circulation. The structure of this ''indirect'' component of the response contrasts with that of the residual component, which is more locally tied to the region of forcing and is baroclinic within the boundary layer while amplifying with height in the free atmosphere. The amplitude of the model response (total, direct, and indirect) is much greater for a positive surface temperature perturbation than a negative one, both for SST and sea ice forcing.

In contrast to the asymmetry in the strength of the response with respect to the polarity of the forcing, the model responds in a nearly linear fashion with respect to the amplitude of the forcing. Figure 4 shows the total, indirect, and direct Z_{500} responses for SST−2.5 and ICE1 that may be compared with their doubled-forcing counterparts SST−5 and ICE2, respectively (recall Fig. 2). The spatial patterns of the responses are similar between the two SST experiments and between the two sea ice experiments, and the amplitudes scale approximately linearly with the magnitude of the forcing. The spatial regression coefficients between the Z_{500} respons-

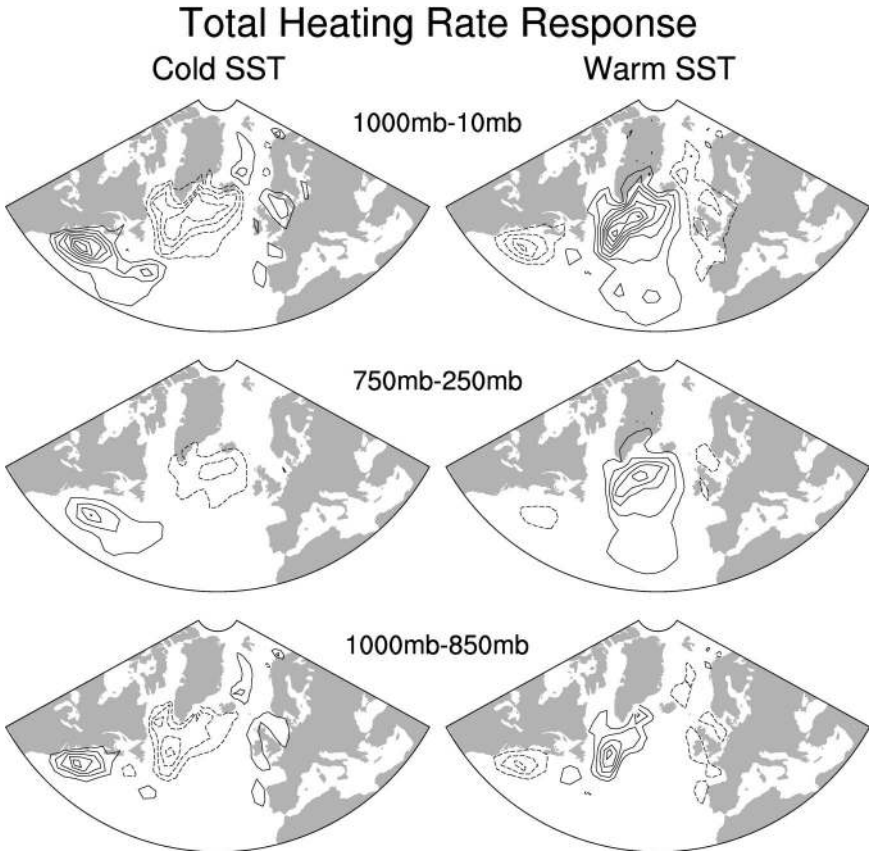

FIG. 5. Vertically integrated heating rate anomalies for (top) the entire depth of the model atmosphere (1000–10 hPa), (bottom) the boundary layer (1000–850 hPa), and (middle) the free troposphere (750–250 hPa) for (left) SST+5 and (right) SST−5. The contour interval is 17.5 W m^{-2} in all panels and the zero contour has been omitted.

es in SST−2.5 and SST−5, a measure of the relative amplitudes of the response patterns are 0.50, 0.46, and 0.49 for the total, indirect, and direct components, respectively, and those between ICE1 and ICE2 are 0.50, 0.54, and 0.38, respectively.

b. Nonlinearity of the response: The role of the vertical distribution of anomalous heating

One factor that may play a role in the stronger model response to positive versus negative SST anomalies is the nonlinear dependence of evaporation upon SST according to the Clausius–Clapeyron relation. Indeed, the magnitude of the latent heat flux anomaly averaged within the 2 K (absolute value) contour of the main SST anomaly center is larger by a factor of 1.4 in SST−5 than SST+5 (see maps in Part I figures). However, this ratio is not large enough to directly account for the approximately three-fold increase in the amplitude of the total response in SST−5 compared to SST+5.

Another factor that may be important is the vertical distribution of the anomalous heating. Figure 5 shows the anomalous heating rate fields integrated over the entire depth of the model atmosphere (1000–10 hPa), the boundary layer (1000–850 hPa), and the free troposphere (750–250 hPa) for SST+5 and −SST+5. In both experiments, the anomalous heating integrated over the depth of the atmosphere is localized to the regions of anomalous SST. There is also anomalous heating over the far eastern North Atlantic that is of opposite sign to that farther west; we speculate this is due to the thermodynamic adjustment of the low-level southwesterly flow to the upstream SST perturbation, as in the experiments of Hall et al. (2001). The magnitude of the anomalous heating in the free troposphere over the central North Atlantic is approximately 2.5 times larger in SST−5 than in SST+5. The anomalous heating patterns within the boundary layer are relatively linear by comparison.

Further detail on the vertical heating distribution is given in Fig. 6, which shows cross sections of the anomalous heating rates in SST−5 and SST+5 averaged over the latitude band (43°–65°N) as a function of longitude and height. The top panel shows the total heating rate anomalies and the lower panels show the individual components that make up the total: the sum of the radiative and vertical diffusion terms, condensational heating in shallow convection, and condensational heat-

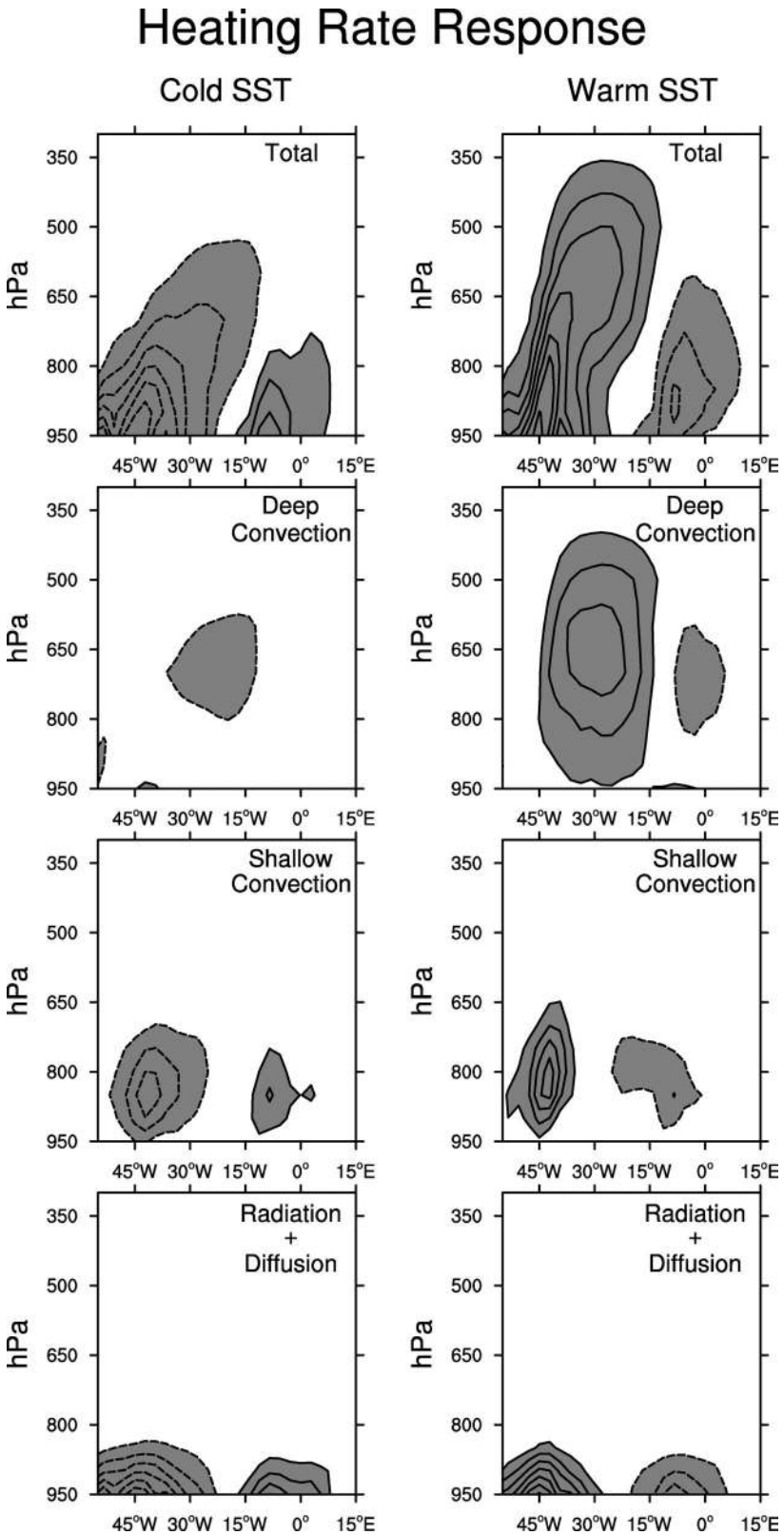

FIG. 6. Vertical cross sections for the lat band 43°–65°N of anomalous heating rates for (left) SST+5 and (right) SST−5 due to (middle top) deep convection, (middle bottom) shallow convection, and (bottom) radiation plus vertical diffusion. (top) The sum of the lower three panels. The contour interval is 0.3 K day^{-1} in all panels; positive (negative) values are indicated by solid (dashed) contours, and the zero contour has been omitted.

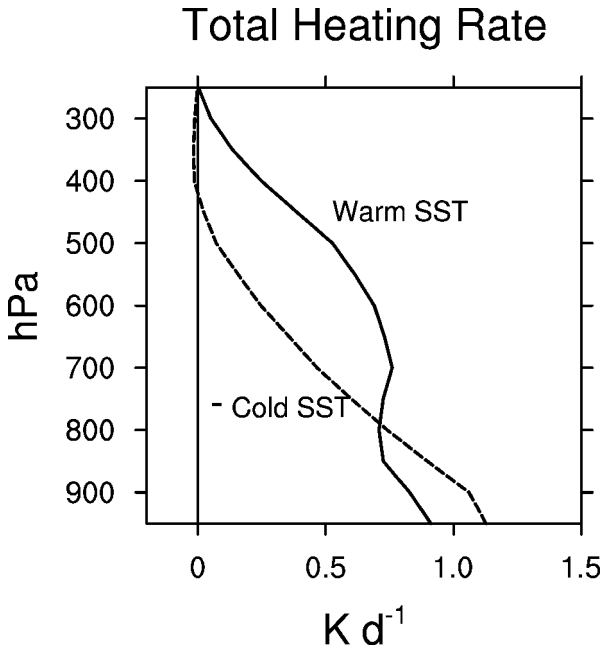

FIG. 7. Vertical profiles of the total anomalous heating rate averaged over the main SST anomaly center (43°–65°N, 50°–30°W) in SST+5 (dashed) and SST−5 (solid). The SST+5 profile has been multiplied by −1.

ing in total precipitation minus that in shallow convection (termed ''deep convection'' in the figure). It is clear that the total heating rate differences in the free atmosphere (e.g., deeper penetration of anomalous heating compared to cooling) are almost entirely due to differences in the deep convective component that peaks in the midtroposphere near 650 hPa. At this level, the magnitude of the anomalous heating due to deep convection is approximately a factor of 3 larger for SST−5 than SST+5. The anomalous heating rates due to shallow convection and radiation plus diffusion are nearly linear by comparison. Figure 6 also shows that the eastward tilt with height apparent in the total heating rate is due to the eastward displacement of deep convection relative to shallow convection.

A summary of the vertical structures of anomalous heating compared to cooling over the main SST anomaly center in SST−5 and SST+5 is given in Fig. 7, which shows area averages for the region (43°–65°N, 50°–30°W; note that the sign has been inverted for SST+5 for easier comparison with SST−5). Although the anomalous heating within the boundary layer is similar in magnitude for the two cases, it is considerably stronger and deeper in the free atmosphere for the positive SST anomaly compared to the negative one. For example, the anomalous heating at 600 hPa is ~0.7 K day^{-1} in SST−5 compared to ~−0.2 K day^{-1} in SST+5, and the level to which the anomalous heating extends is ~300 hPa in SST−5 compared to ~500 hPa in SST+5.

Given the stronger and deeper anomalous heating in SST−5 compared to the anomalous cooling in SST+5, it is now evident why the direct component of the geopotential height response in SST−5 amplifies with height at a considerably greater rate than that in SST+5 (recall Fig. 3) because the thickness between two geopotential height surfaces must be proportional to the temperature anomalies in the layer. The degree to which the vertical profile of the anomalous heating or cooling affects the strength of the *indirect* response cannot be definitively answered without a more complete understanding of the dynamical mechanisms responsible for the leading mode of internal variability in the model. However, qualitatively we expect that a deeper heating profile will project more strongly onto the equivalent barotropic vertical structure of the leading internal mode of variability, thus exciting it more efficiently. In this context, Hall et al. (2001) have examined the sensitivity of the response of a simplified AGCM to different idealized vertical profiles of midlatitude heating and find that ''the pattern of the global response is not very sensitive to the changes in the shallow heating profile, but as the heating becomes deeper the response is stronger both locally and in the equivalent barotropic teleconnections.'' Indeed, we find that the indirect response is approximately 3 times larger in magnitude for SST−5 than SST+5, a factor that is similar to the difference in strength of the anomalous heating above the boundary layer in the two experiments (recall Figs. 5–7).

Of course, the anomalous heating pattern itself may be affected by the circulation response, in particular the indirect component. To examine this possibility, we decomposed the vertically integrated heating rate response in SST−5 into indirect and direct components by regression upon the leading Z_{500} PC time series in the control run [this time series is highly correlated (r = 0.86) with the leading PC of the vertically integrated heating field in the control run]. The projection onto the leading internal mode (Fig. 8) exhibits a north–south dipole in the Atlantic, with enhanced heating along 40°–50°N and diminished heating along 60°–70°N associated with a southward shift of the mean westerly jet (see also Fig. 10a in Part I). However, this indirect component is approximately a factor of 5 weaker than the total response, so that the total heating rate response is dominated by the direct component, unlike the case for geopotential height (recall Fig. 2). Thus, the indirect circulation response does not substantially impact the total vertically integrated heating response. This result indicates that other processes besides heating, such as eddy momentum fluxes, are important for the maintenance of the internally generated variability, consistent with previous studies (cf. Ting and Lau 1993 and Fig. 14a in Part I). Analogous results are obtained for SST+5 and ICE2 (not shown).

Why does the anomalous heating extend so much higher in the warm SST experiment compared to the cold one? The answer may be simply that cooling from below is an inherently stabilizing process while heating

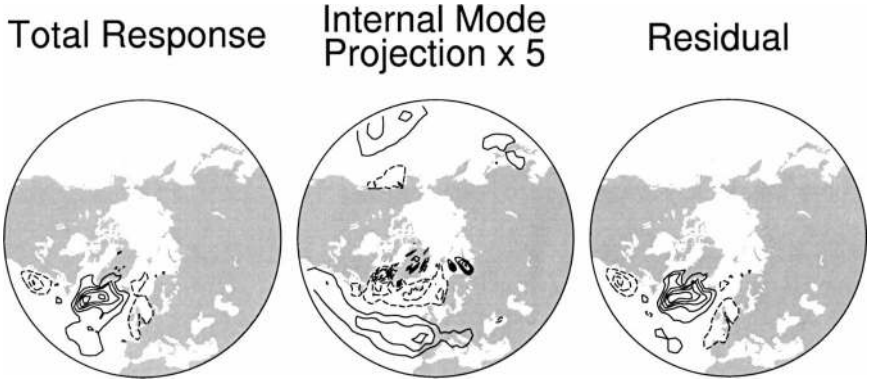

FIG. 8. As in Fig. 2 but for the vertically integrated total anomalous heating rate in SST−5. The contour interval is 15 W m^{-2} in all panels (the values in the middle panel have been multiplied by 5) and the zero contour has been omitted.

from below is a destabilizing one, conducive to convective overturning and deeper vertical penetration. In support of this notion, we show mean vertical temperature profiles averaged over the main SST anomaly center from the control, SST−5, and SST+5 experiments (Fig. 9). It is clear that the positive temperature perturbation is sufficiently buoyant relative to the control run lapse rate that it can extend into the upper troposphere while the negative one is mainly confined to the lower troposphere.

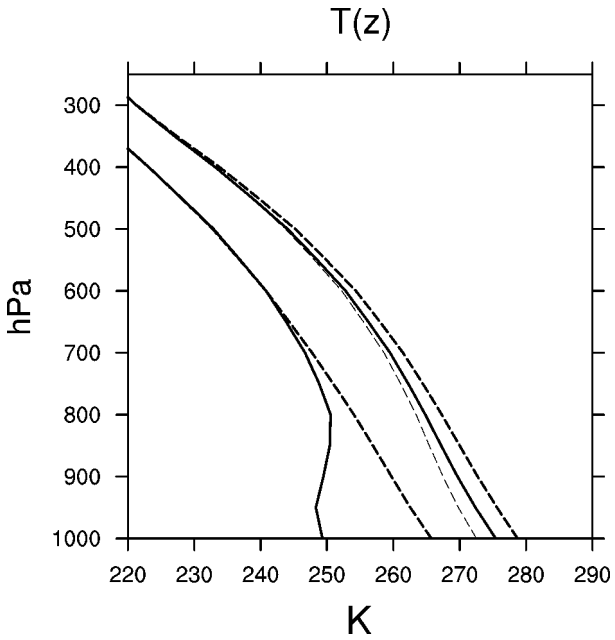

FIG. 9. Long-term mean winter temperature profiles. The two coldest profiles are for the Greenland Sea region (74°–85°N, 20°W–100°E) from the control run (solid) and ICE2 (dashed). The three warmest profiles are for the north-central Atlantic (43°–65°N, 50°–30°W) from the control run (solid), SST+5 (thin dashed), and SST−5 (thick dashed).

c. Sea ice versus SST forcing

In the previous section, we hypothesized that the stronger model response to positive versus negative SST anomalies is mainly due to the deeper penetration of anomalous heating compared to cooling. Does this argument apply to the sea ice experiments, and in particular, does it explain why the response to reduced ice cover in the Greenland Sea (e.g., surface warming) is so much larger than that to enhanced ice cover in the Labrador Sea (e.g., surface cooling; not shown but see Part I)? Figure 10 shows the anomalous heating rate fields integrated over the entire depth of the model atmosphere, the boundary layer, and the free troposphere for the ICE2 experiment. The anomalous heating rate integrated over the depth of the atmosphere exhibits large negative (positive) values over the enhanced (reduced) ice cover in the Labrador (Greenland) Sea, with weaker values of opposite sign directly downstream due to the modification of the air mass as it encounters open water (see Part I). Peak values associated with the ice cover changes are ~ -300 W m^{-2} over the Labrador Sea and ~ 150 W m^{-2} over the Greenland Sea (the higher values in the Labrador Sea may be due to the stronger cross-ice component of the near-surface winds that enhances the surface turbulent energy flux anomaly; not shown). These peak values are considerably larger than those in the SST anomaly experiments, although they are restricted to a smaller area. In contrast to the results for SST−5, the anomalous heating over the Greenland Sea is confined almost entirely to the lower troposphere. We note that the shallowness of the anomalous heating profile over the Greenland Sea is consistent with the vertical structure of the direct response (recall Fig. 3a) in that the anomalous ridge directly over the reduced ice cover does not amplify above $\sim$700 hPa.

The results shown in Fig. 10 raise two questions: 1) why does the anomalous heating associated with reduced ice extent in the Greenland Sea not penetrate as deeply as that associated with a warm SST anomaly in

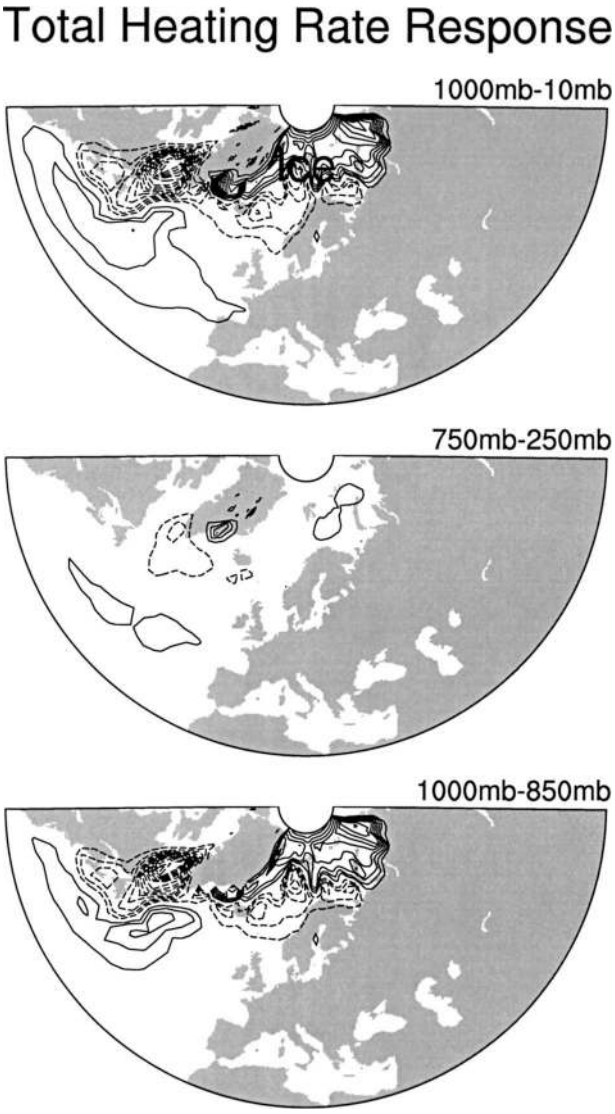

FIG. 10. As in Fig. 5 but for ICE2.

the North Atlantic, and 2) if the anomalous heating over the Greenland Sea is so shallow, why is the indirect component of the geopotential height response so large (as large as the response in SST−5)? The mean vertical temperature profiles over the Greenland Sea (74°–85°N, 20°W–100°E) in the control and ICE2 experiments, shown in Fig. 9, provides some insight into the first question. When sea ice is present (in the control run), the lower troposphere is nearly isothermal and consequently, very large positive surface temperature perturbations are needed to overcome the strong static stability. Indeed, a surface temperature anomaly of 17 K (ICE2-minus-control) is only large enough to penetrate to ~700 hPa. In contrast, a surface temperature perturbation of only 4 K in SST−5 is sufficient to penetrate to ~350 hPa due to the weaker stratification over the ice-free North Atlantic (Fig. 9). Thus, we speculate that the mean static stability in the region of the surface temperature perturbation plays a decisive role in how deep the anomalous heating can penetrate.

Given that the anomalous heating over the Greenland Sea in the ICE2 experiment does not penetrate as deeply as that over the North Atlantic in SST−5, why are the indirect responses in free atmosphere comparable in the two experiments? Put another way, why is the leading mode of internal variability excited so strongly in the ICE2 (and ICEGRN) experiment? Although we do not have a definitive answer to this question, we speculate that the ice anomaly in the Greenland Sea may be located in a region to which the model's internal variability is particularly sensitive. In this context, we note that the Greenland Sea ice perturbation is broad in zonal extent and located near the Arctic center of action of the leading Z_{500} EOF in the control simulation, perhaps resulting in an efficient projection upon the spatial pattern of the dominant mode of internal variability. Another possible factor is the interaction of the flow in the forcing region with the upstream topographic barrier of Greenland, which may result in a strong projection upon the internal mode. Further work is planned to investigate these issues.

4. Summary and further discussion

We have decomposed the simulated total geopotential height responses to North Atlantic SST and sea ice cover anomalies into a portion that projects onto the leading mode of internal variability (the indirect response) and the residual from that projection (the direct response). We suggest that this empirical decomposition yields physically meaningful patterns with distinctive horizontal and vertical structures, as discussed below.

a. The direct response

The direct component of the response to a positive North Atlantic SST anomaly (SST−5) exhibits a baroclinic structure in the vertical, with a surface trough directly over the SST anomaly and an equivalent barotropic ridge in the free atmosphere over and slightly downstream of the SST anomaly. This structure is qualitatively consistent with simple theoretical models of the linear baroclinic response to extratropical thermal forcing (see, e.g., the review by Kushnir et al. 2002). A similar pattern of opposite sign is found for the direct response to a negative SST anomaly (SST+5), but the amplitude is weaker by a factor of 2–3. The weaker response in SST+5 than SST−5 may be a result of the reduced magnitude and vertical extent of the anomalous cooling associated with a negative SST anomaly compared to anomalous heating associated with a positive one. We postulate that the shallower vertical extent of a negative heating anomaly compared to a positive one is due to the stabilizing effect of surface cooling versus the destabilizing effect of surface heating. Unlike the

asymmetry in the strength of the direct response to positive versus negative SST forcing, the direct response is approximately linearly proportional to the magnitude of the imposed SST anomaly.

The direct response to reduced sea ice cover in the Greenland Sea is analogous to the direct response in SST−5 except that the anomalous ridge in the free atmosphere does not penetrate as deeply (e.g., does not amplify with height above ~700 hPa). We suggest that this is due to the more limited vertical extent of the anomalous heating resulting from the higher mean static stability in the lower troposphere associated with the presence of sea ice in the control run. As in the SST forcing experiments, the direct response to anomalous sea ice cover is nonlinear with respect to the polarity of the forcing and approximately linear with respect to the amplitude of the forcing.

b. The indirect response

The indirect response, or the component of the response that projects onto the leading mode of internal variability, dominates the total geopotential height response in both SST−5 and ICE2. Like the direct response, the magnitude of the indirect response scales linearly with the amplitude of the forcing but nonlinearly with the sign of the forcing. Unlike the direct response, the horizontal structure of the indirect response is hemispheric in scale, resembling the North Atlantic Oscillation or Northern Hemisphere annular mode, and the vertical structure is approximately equivalent barotropic from the surface to the tropopause.

Many outstanding issues regarding the indirect response remain to be investigated, including an understanding of the dynamical processes responsible for the leading internal mode of variability including essential interactions between the transient and stationary eddies and the mean flow, the factors that determine the polarity of the indirect response and the relative strengths of the indirect and direct responses, and the mechanisms responsible for the nonlinear behavior of the indirect response with respect to the sign of the forcing. Recently, Peng et al. (2003) have proposed that nonlinear interactions between the anomalous heating and eddy-induced components of the flow can lead to asymmetries in the response to positive versus negative SST anomalies. Idealized experiments are planned to examine these issues, including the sensitivity of the indirect response to the location and polarity of the forcing and to the vertical profile of the associated anomalous heating, as well as possible nonlinear interactions between the anomalous heating and eddy forcing.

Acknowledgments. We wish to thank Dr. Michael Alexander for useful discussions during the course of this work and the three anonymous reviewers for helpful comments. We are also grateful to Dr. Christophe Cassou for his technical assistance. GM was supported by NOAA OGP under Grant NA96GP0420.

REFERENCES

Deser, C., J. E. Walsh, and M. S. Timlin, 2000: Arctic sea ice variability in the context of recent atmospheric circulation trends. *J. Climate,* **13,** 617–633.

Hall, N. M. J., J. Derome, and H. Lin, 2001: The extratropical signal generated by a midlatitude SST anomaly. Part I: Sensitivity at equilibrium. *J. Climate,* **14,** 2035–2053.

Kushner, P., I. Held, and T. L. Delworth, 2001: Southern Hemisphere atmospheric circulation response to global warming. *J. Climate,* **14,** 2238–2249.

Kushnir, Y., W. A. Robinson, I. Blade, N. M. J. Hall, S. Peng, and R. Sutton, 2002: Atmospheric GCM response to extratropical SST anomalies: Synthesis and evaluation. *J. Climate,* **15,** 2233–2256.

Magnusdottir, G., C. Deser, and R. Saravanan, 2004: The effects of North Atlantic SST and sea-ice anomalies on the winter circulation in CCM3. Part I: Main features and storm track characteristics of the response. *J. Climate,* **17,** 857–876.

Peng, S., and W. A. Robinson, 2001: Relationships between atmospheric internal variability and the responses to an extratropical SST anomaly. *J. Climate,* **14,** 2943–2959.

——, ——, and S. Li, 2003: Mechanisms for the linear and nonlinear NAO responses to the North Atlantic SST tripole. *J. Climate,* **16,** 1987–2004.

Seager, R., Y. Kushnir, M. Visbeck, N. Naik, J. Miller, G. Krahmann, and H. Cullen, 2000: Causes of Atlantic Ocean climate variability between 1958 and 1998. *J. Climate,* **13,** 2845–2862.

Ting, M., and N.-C. Lau, 1993: A diagnostic and modeling study of the monthly mean wintertime anomalies appearing in a 100-year GCM experiment. *J. Atmos. Sci.,* **50,** 2845–2867.

Wallace, J. M., 2000: North Atlantic Oscillation/annular mode: Two paradigms—One phenomenon. *Quart. J. Roy. Meteor. Soc.,* **126,** 791–805.